Composites Science and Technology 145 (2017) 105–113

Contents lists available at ScienceDirect

Composites Science and Technology

journal homepage: http://www.elsevier.com/locate/compscitech

Dielectric response and breakdown behavior of polymer-ceramic nanocomposites: The effect of nanoparticle distribution

Ziming Cai [a], Xiaohui Wang [a, *], Bingcheng Luo [a], Wei Hong [b, c], Longwen Wu [a], Longtu Li [a, **]

[a] State Key Laboratory of New Ceramics and Fine Processing, School of Materials Science and Engineering, Tsinghua University, Beijing, 100084, PR China
[b] Department of Aerospace Engineering, Iowa State University, Ames, IA, 50010, USA
[c] Global Station for Soft Matter, Global Institution for Collaborative Research and Education, Hokkaido University, Sapporo, Japan

ARTICLE INFO

Article history:
Received 25 January 2017
Received in revised form
22 March 2017
Accepted 28 March 2017
Available online 29 March 2017

Keywords:
Distribution
Nanocomposite
Dielectric response
Breakdown strength
Size effect

ABSTRACT

Polymer-ceramic nanocomposites play an essential role in the application of pulsed power system, due to their ultrahigh power density and fast charging–discharging capability. It is very promising for them to be applied in energy storage capacitors and hybrid electric vehicles for the recent progressing in the improving energy density. The volume fraction, morphology, size, aspect ratio and distribution of ceramic particles have been reported to have significant effect on the dielectric response and breakdown strength of nanocomposites, which are two main factors that determine the energy density of nanocomposites. In this study, we introduce a quantified method to describe the distribution of ceramic nanoparticles in polymer matrix, then focus on the effect of nanoparticles distribution on dielectric response and breakdown strength of nanocomposites through finite element method and phase field method. Results indicate that the non-uniform distribution of ceramic nanoparticles will aggravate the concentration of local electric field, thus slightly enhance the dielectric response but seriously decrease the breakdown strength of nanocomposites. To verify the size effect of ceramic particles on breakdown strength of nanocomposites, three types of well distributed nanoparticles with different diameter of particles have also been calculated using the same method.

1. Introduction

Polymer-ceramic nanoparticles are critical for the application in pulsed power system, due to their fast charging-discharging capability and high power density [1–3]. Recently, growing environmental problem requires a large amount of cleaner energy together with a new, environmentally friendly and low-cost energy storage devices. In principle, dielectric permittivity and breakdown voltage are two major factors that determine the energy storage density of these devices, which can be written as

$$J = \int_0^{D_{max}} EdD, \quad (1)$$

where J is energy storage density, E is electric field strength, D is dielectric displacement, and D_{max} is the dielectric displacement under saturated electric field strength. Polymer-ceramic nanoparticles show superior advantages to all other candidates, since that polymers are known for their high breakdown strength, meanwhile ceramic can obtain high polarization [4–9]. A great deal of attention has been paid to fabricate such high energy density nanocomposites featured with high permittivity, high dielectric breakdown strength, low dielectric loss and long cycle life [10–19]. These nanocomposites are typically filled with ferroelectric ceramics such as $BaTiO_3$, $BaSrTiO_3$ [20–24] or nonferroelectric fillers like boron nitride, graphene oxide [25–27]. A maximum energy density of >30 J/cm^3 has been achieved in P(VDF-HFP)/BTO@TO_nfs nanocomposites [28]. The volume fraction, morphology, size, aspect ratio and distribution of ceramic particles have been reported to have significant effect on the dielectric response and breakdown strength of nanocomposites. Among all these

* Corresponding author.
** Corresponding author.
E-mail addresses: wxh@mail.tsinghua.edu.cn (X. Wang), llt-dms@mail.tsinghua.edu.cn (L. Li).

http://dx.doi.org/10.1016/j.compscitech.2017.03.039
0266-3538/

characters, the effect of volume fraction, morphology, size, aspect ratio and qualitative distribution of ceramic particles on dielectric response and breakdown strength of polymer-ceramic nanoparticles has been widely studied both experimentally and numerically [29–36]. However, the study on quantified description of ceramic particles in polymer matrix is quite rare [37].

In this study, we introduce a quantified method to describe the distribution of ceramic nanoparticles in polymer matrix based on complete spatial randomness (CSR) test [38]. CSR test is a pretty mature theory in the field of statistics, which can be achieved by different approaches, namely goodness-of-fit test [39], means of angles [40], Bivariate Cramer-von Mises type of test [41], minimal spanning tree [42], simple Monte Carlo test and Clark-Evans test [43]. Here, we choose a straightforward method called Clark-Evans test based on measurement of neatest neighbor distance of each nanoparticles [44]. Five different distribution of ceramic nanoparticles has been generated through MATLAB R2016a and then, the Clark-Evans test was used to quantify each distribution. After that, the effect of these five quantified distribution of ceramic particles on dielectric response and breakdown strength of nanocomposites are respectively calculated through finite element method and phase field method both in COMSOL Multiphysics 5.2a. To verify the size effect of ceramic particles on breakdown strength of nanocomposites, three types of well distributed nanoparticles with different diameter of particles have also been calculated using the same method above.

2. Fundamental theories

2.1. Clark-Evans test [45]

Consider a square region of nanoparticles marked as R. Assume that the ceramic particles occupy 2D circular domains of approximately the same size. As sketched in Fig. 1, for any pair of circular particles centered as $s = (s_1, s_2)$ and $v = (v_1, v_2)$ in R, we denote the distance between s and v by

$$\mathrm{d}(s, v) = \sqrt{(s_1 - v_1)^2 + (s_2 - v_2)^2}, \tag{2}$$

If there are n particles in R, we can obtain n-1 distances for each circle.

The minimum distance is then defined as the nearest neighbor distance (nn-distance) for each particle. Finally, we obtain n nn-distances, denoted as d_i ($i = 1,...,n$). According to the Skellam's statistic, independent sums of identically distribute random variables

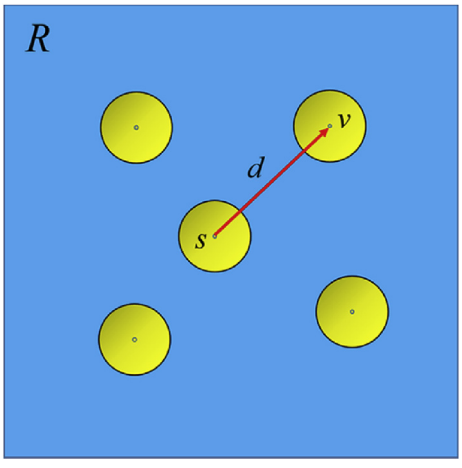

Fig. 1. Schematic diagram of nano-ceramic particles in polymer matrix nanocomposite.

are approximately normally distributed. Hence following the Central Limit Theorem, the most common CSR test Hypothesis base on nn-distances involves a normal approximation to the sample mean of D, as defined by

$$\overline{D}_n = \frac{1}{n}\Sigma_{i=1}^{n} D_i, \tag{3}$$

We can eventually achieve the normal distribution of $\overline{D}_n$ based on statistic theories.

$$\overline{D}_n \sim N\left(\frac{1}{2\sqrt{\lambda}}, \frac{4-\pi}{n(4\lambda\pi)}\right), \tag{4}$$

where λ is the particle density, defined as $n/a(R)$, where n is the number of particles and $a(R)$ represent the area of R. Note that, $X \sim N(\mu, \sigma^2)$ represents that a random variable X obeys the normal distribution with μ as mean value and σ^2 as variance. Thus, the standardized sample mean under the CSR Hypothesis by

$$z_n = \frac{\overline{D}n - \left[1\Big/\left(2\sqrt{\lambda}\right)\right]}{\sqrt{(4-\pi)/(n4\pi\lambda)}}, \tag{5}$$

then it follows at once from (4) that under CSR,

$$z_n \sim N(0, 1). \tag{6}$$

Unfortunately, if we use all these n nn-distance to construct the CSR Hypothesis test based on this distribution, a trouble would be encountered since there could be two same nn-distance ($d_i = d_j$), which violates the independence assumption. The solution is that we choose a subset of nn-distance values that contain no common circles. The way to select such an independent subset is complicated but practicable. Here, we simply assume that some independent subset ($d_1,...,d_m$) of these nn-distance has been selected with $m < n$. At last, given this sample, we can construct a sample mean value,

$$\overline{d}_m = \frac{1}{m}\Sigma_{i=1}^{m} d_i, \tag{7}$$

and use this to construct the test of CSR.

2.2. Landau theory on ferroelectric ceramic particles

In this work, the side length (L) of selected square region (R) of nanocomposites is set to 1 μm. The most widely used ferroelectric ceramic particles barium titanate (BT) was taken as the example of nanoparticle fillers in our following calculation. The polymer matrix nanocomposites can be taken as a ferroelectric-dielectric system, for which the polymer matrix can be seen as linear dielectric, while the ceramic nanofillers are considered non-linear ferroelectric, of which behavior can be described through Landau's theory of phase transformation. A Landau expansion up to the sixth order was chosen to demonstrate the nonlinear dielectric response of BT with the Landau potential (ΔG) [46], which reads

$$\Delta G = \frac{1}{2}\alpha P^2 + \frac{1}{4}\beta P^4 + \frac{1}{6}\gamma P^6 - EP, \tag{8}$$

where P is the polarization, E is the applied electric field, and α, β and γ are the dielectric stiffness coefficients [46]. In stress-free polymer matrix, the equation of state of the electric field dependence of polarization and the dielectric response and its stability parallel to the applied electric field are given by Ref. [47].

$$\frac{\partial \Delta G}{\partial P} = 0 = \alpha P + \beta P^3 + \gamma P^5 - E, \tag{9}$$

$$\varepsilon_r(E) = \frac{1}{\varepsilon_0(\alpha + 3\beta P^2 + 5\gamma P^4)}, \tag{10}$$

$$\eta(E) = \frac{\varepsilon_r(E) - \varepsilon_r(E=0)}{\varepsilon_r(E=0)}. \tag{11}$$

At room temperature, the dielectric response of BT can be calculated numerically, as shown in Fig. 2, which exhibits the well-known butterfly-like ferroelectric response and the hysteresis is ignored for simplicity [48].

The dielectric response of nanocomposites is simulated using COMSOL Multiphysics. The dielectric permittivity of linear polymer matrix is separately set as 12, 50 and 100 to verify the influence of matrix on the dielectric response of nanocomposites. The effective dielectric permittivity can be calculated from Ref. [48].

$$\varepsilon_r = \mathrm{d}\frac{\int D \cdot E \mathrm{d}V}{\varepsilon_0 A U^2}. \tag{12}$$

2.3. Phase field method on dielectric breakdown

The study of the dielectric breakdown process of nanocomposites follows closely the phase field model developed in Refs. [49,50], by drawing an analogy between dielectric breakdown and mechanical fracture. A scalar phase field $s(x, t)$ is introduced to characterize the breakdown process of a dielectric medium. The value of s varies from 1 to 0, which respectively represent the intact state and the fully damaged state. The fully damaged material becomes conductive. Numerically, a large but finite permittivity ε_0/η is taken for such material part, where ε_0 is the initial permittivity and η is a small enough number. For any other intermediate state of nanocomposites, the permittivity is interpolated by

$$\varepsilon(s) = \frac{\varepsilon_0}{f(s) + \eta}, \tag{13}$$

where $f(s) = 4s^3 - 3s^4$. Breakdown happens if the process decreases the total potential energy of the system

$$\Pi[s, \phi] = \int_{\Omega} [W_{es}(E, s) + W_d(s) + W_i(\nabla s)] \mathrm{d}V, \tag{14}$$

where $W_{es}(E, s) = -\frac{\varepsilon}{2} E \cdot E$ is the complementary electrostatic energy per unit volume, $W_d(s) = W_c[1 - f(s)]$ is the breakdown energy function with W_c representing the critical density of electrostatic energy, $W_i(\nabla s) = \frac{\Gamma}{4} \nabla s \cdot \nabla s$ is the gradient energy term to regulate sharp phase boundaries. It is worth noting that the material parameter Γ is approximately the breakdown energy [41]. According to linear kinetic law: $\partial s/\partial t = -m\delta\Pi/\delta s$, the evolution equation for breakdown variable s can be achieved after substituting in detailed forms of the energy functions:

$$\frac{1}{m}\frac{\partial s}{\partial t} = \frac{\varepsilon'(s)}{2} \nabla\phi \cdot \nabla\phi + W_c f'(s) + \frac{\Gamma}{2} \nabla^2 s. \tag{15}$$

Here, mobility m is a material parameter that features the speed of breakdown propagation in nanocomposites. Finally, the normalized governing equations of dimensionless form can be written as:

$$\overline{\nabla} \cdot \left[\frac{1}{f(s) + \eta} \overline{\nabla}\, \overline{\phi} \right] = 0, \tag{16}$$

$$\frac{\partial s}{\partial \overline{t}} = -\frac{f'(s)}{2[f(s) + \eta]^2} \overline{\nabla}\, \overline{\phi} \cdot \overline{\nabla}\, \overline{\phi} + f'(s) + \frac{1}{2} \overline{\nabla}^2 s, \tag{17}$$

in which the corresponding quantities are symbolized with overbars. While the above described model considers only linear dielectrics, here in this study we add the nonlinear performance of nanoceramic by normalizing Eqs. (9) and (10) into:

$$\alpha \overline{P} + \beta \overline{P}^3 + \gamma \overline{P}^5 - \overline{E} = 0, \tag{18}$$

$$\varepsilon_r(\overline{E}) = \frac{1}{\varepsilon_0\left(\alpha + 3\beta \overline{P}^2 + 5\gamma \overline{P}^4\right)}. \tag{19}$$

With the focus mainly on the mechanism study of dielectric response and breakdown process, all simulations are carried out in two-dimensional (2D) domains.

3. Results and discussion

3.1. Quantified distribution description of ceramic nanoparticles based on Clark-Evans test

Five different random distributions have been generated through MATLAB. Each case contains 100 BT nanoparticles in a 1 μm × 1 μm square region of nanocomposites. The five cases marked as I to V correspond to Fig. 3(a)–(e). The diameter of the BT particles used is 40 *nm*. Afterward, the Clark-Evans test was used to quantify each distribution. At first, we can obtain 100 nn-distance corresponding to each circle of every different distribution. A random sub set of 50 nn-distance is chosen from 100 nn-distance in each case to avoid the dependence among circles through MATLAB. The mean value of these 50 nn-distance ($\overline{d}_m$) and the standardized sample mean of nn-distance (z_m) are calculated based on Clark-Evans test as shown in Table 1. Here, z_m is the quantified criterion to evaluate the distribution. The larger the z_m, the more uniform the distribution. Furthermore, we can define that if the value of z_m is larger than 10, then such case can be seen as a pretty uniform distribution. Compared Table 1 with Fig. 3(a)–(e), the results of Clark-Evans test show a good consistent with our visual perception.

3.2. Dielectric response and stability against five different random distribution cases

Consider the nonlinear ferroelectric behavior of BT, we

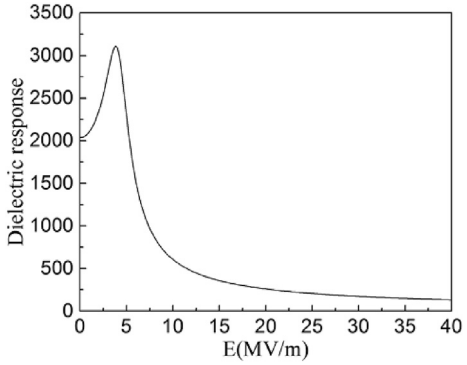

Fig. 2. Dielectric response of BT ceramic as a function of applied electric field.

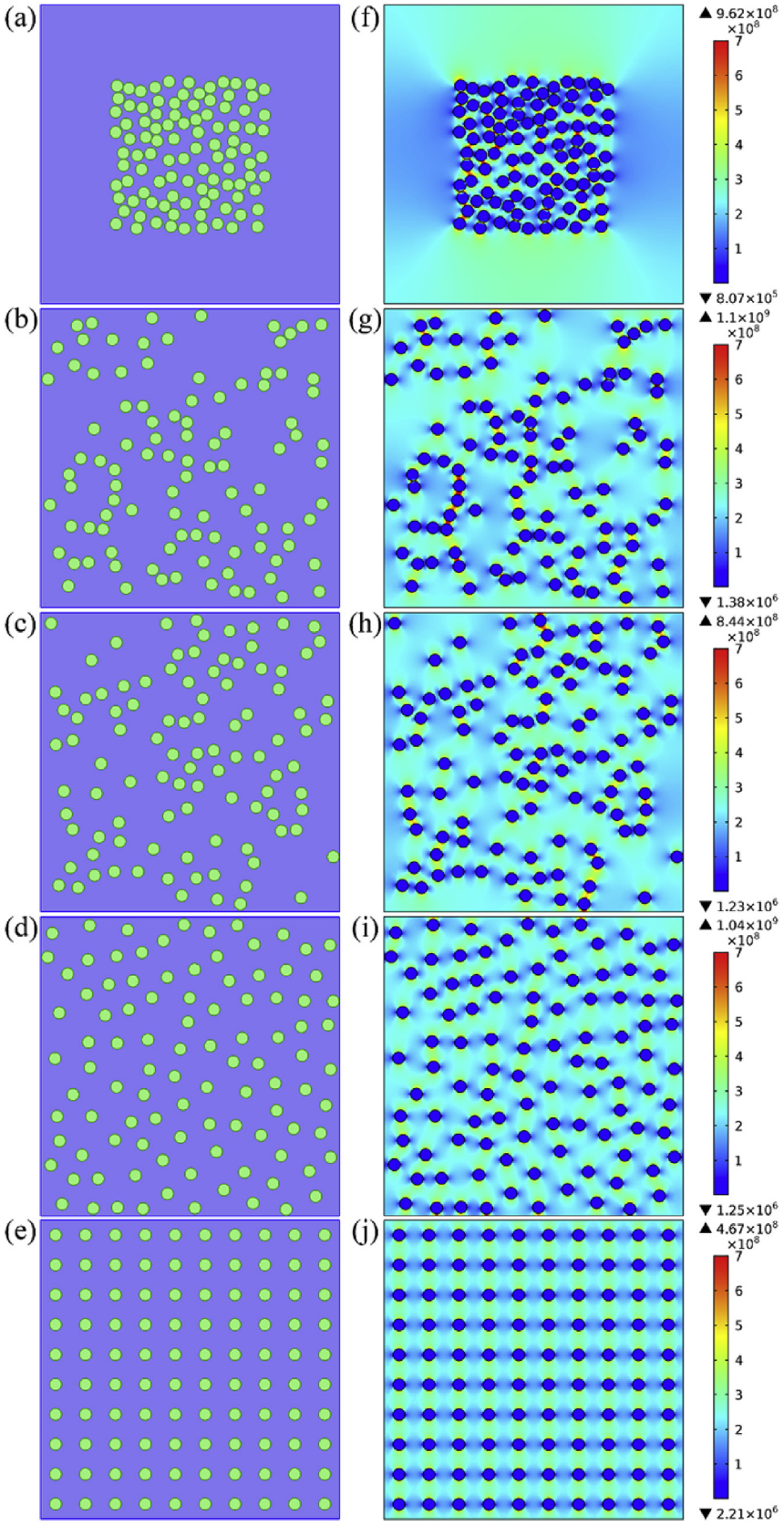

Fig. 3. Five different random distributions of ceramic particles in polymer matrix from (a) to (e); (f) to (j) The distribution of electric field strength (in the unit V/m) corresponding to each random distribution under the applied electric field of 200 MV/m.

Table 1
The mean value of 50 nn-distance ($\bar{d}_m$) and the standardized sample mean of nn-distance (z_m) of each case.

case	$\bar{d}_m$	z_m
I	0.44	−1.51
II	0.65	3.99
III	0.68	4.93
IV	0.88	10.32
V	1	13.51

implement equations (9) and (10) into COMSOL Multiphysics. Combining equations (11) and (12), the effective dielectric response and stability of nanocomposites can be calculated. As mentioned in 2.2, The dielectric permittivity of linear polymer matrix of 12, 50 and 100 is separately calculated to verify the influence of matrix on the dielectric response of nanocomposites, and results are shown in Fig. 4.

From Fig. 4(a)–(c), we can summarize that along the distribution of BT getting more non-uniform, the dielectric response of nanocomposite on the contrary increase slightly. It is easy to understand that as the distribution of BT becomes worse, the concentration of local electric field aggravates a lot, result in a larger electric displacement as shown in Fig. 3(f)–(j). According to the origin equation (1), one can figure out that for an undamaged dielectric material, a larger D and E will enhance the total energy of material, thus shows a higher dielectric response [51]. However, this local electric field concentration induced higher dielectric response in turn will seriously reduce the breakdown resistance, since the dielectric breakdown will start at the certain point where the local electric field concentrates most. A further study on breakdown process will be discussed in section 3.3. If we just take two ceramic particles into consideration, the specific electrostatic interaction between these two particles can be simulated. We change the distance of two particles only with other geometry, material properties and applied electric field remained unchanged. The change of electric field and electric displacement against distance of particles can be clearly seen in Fig. 5. It is clear that as the distance between ceramic particles reduces, the local electric field and electric displacement will be amplified, which is the more detailed supplement for the results shown in Fig. 4 (a) to (c).

The effective dielectric response is affected more seriously when the distribution of BT is worse, which is indicated in Fig. 4 (d) to (f). The worse distribution of BT aggravates the local electric field, which leads that the nanocomposites perform more similar to the filled BT particles. However, the nanocomposites with well distributed BT particles can hold the dielectric stability up to a

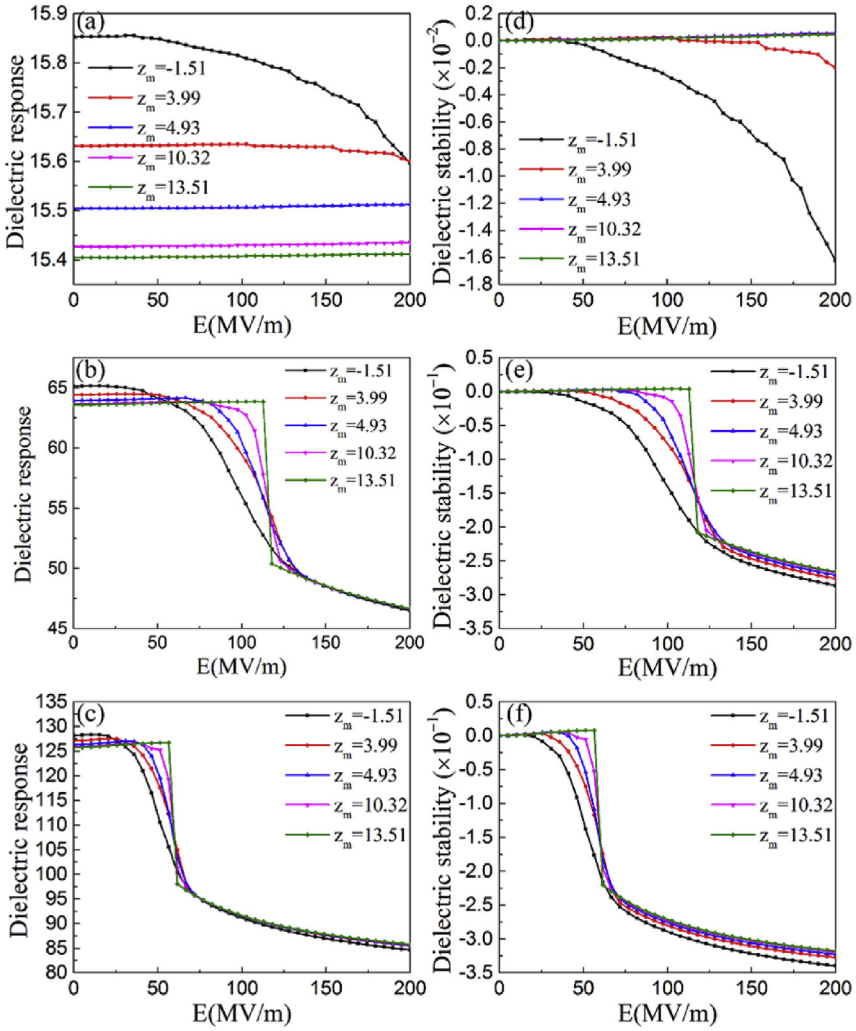

Fig. 4. (a) to (c) The effective dielectric response of nanocomposites. (d) to (f) The dielectric stability of nanocomposites with the matrix permittivity: (a) and (d) 12, (b) and (e) 50, (c) and (f) 100.

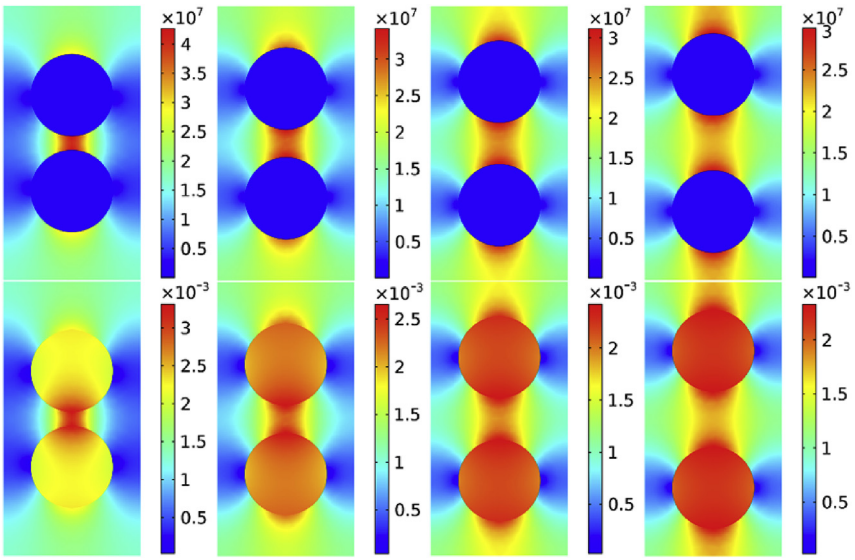

Fig. 5. The distribution of electric field (upper four pictures, unit: V/m) and electric displacement field (under four pictures, unit: C/m^2) against distance change between ceramic particles.

higher level of applied electric field and then drop sharply at a critical applied electric field as seen in Fig. 4 (d) to (f).

3.3. Dielectric breakdown resistance against five different random distribution cases

The normalized governing equations (16) and (17) of phase field together with normalized dielectric equations (18) and (19) based on Landau theory are implemented into COMSOL Multiphysics to simulate the dielectric breakdown process. All results are normalized by the material constants of the matrix.

For distribution case I, of which z_m equals −1.51, the detailed damage evolution process of the nanocomposite with a short field concentrator is shown by the three snapshots in Fig. 6(a)–(c). Inspired by the standard fracture mechanics testing procedures, a conductive field concentrator is introduced to overcome the effect of random defects. The conductive channel is shown by the blue region in Fig. 6(a)–(c). It could be seen that the breakdown initiates at the closest points between neighboring BT particles, where the electric field is the most concentrated. The breakdown energy of BT particles is smaller than that of polymer matrix, the propagation of conductive channel will then pass through BT particles. When the

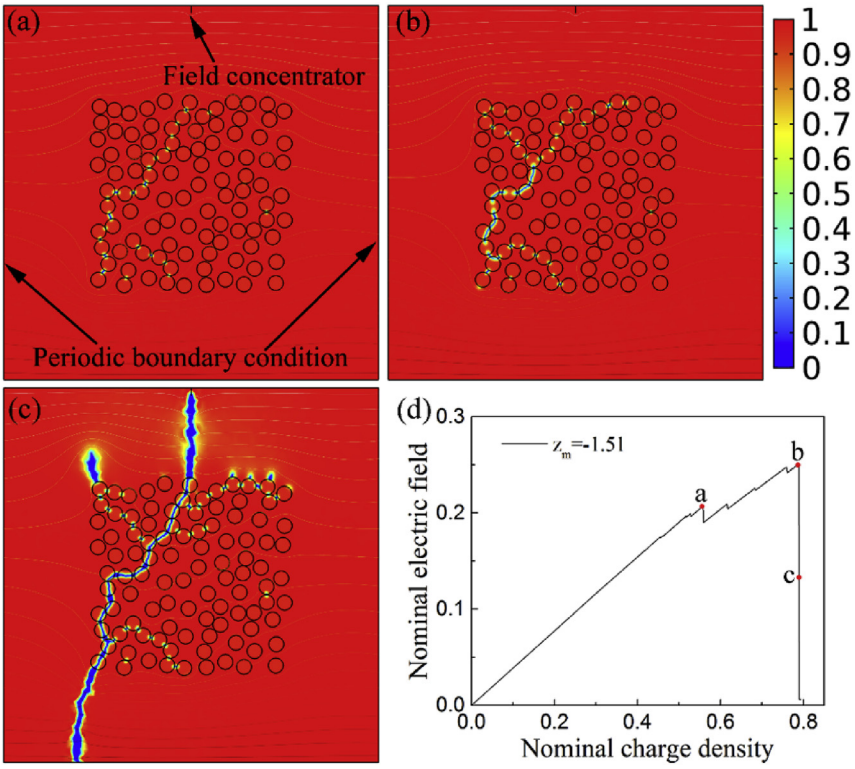

Fig. 6. (a) to (c) Snapshots of the breakdown process of nanocomposite of case I with a short field concentrator, indicating the evolution of the breakdown channel. (a), (b) and (c) correspond to the three dots a, b and c on (d). (d) The nominal field-charge-density relation of case I. The contour lines are the equipotential lines of the then-current electric field.

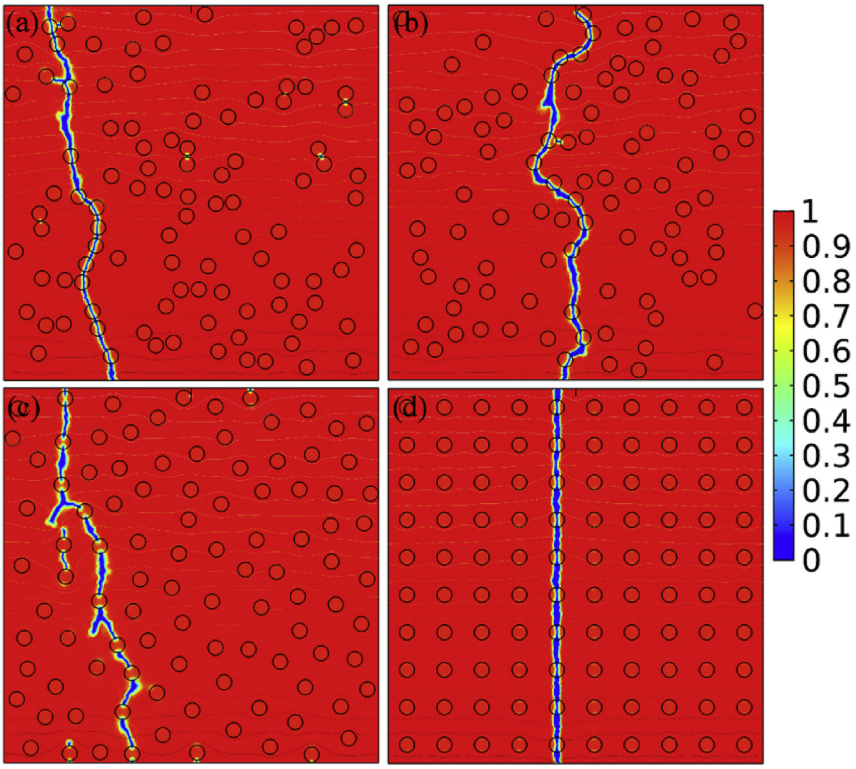

Fig. 7. The breakdown path featured by different standardized sample mean (z_m): (a) $z_m = 3.99$, (b) $z_m = 4.93$, (c) $z_m = 10.32$, (d) $z_m = 13.51$. The contour lines are the equipotential lines of the then-current electric field.

electric field reaches a critical value, the conductive channel will percolate and suddenly penetrate throughout nanocomposite. Such a breakdown process can also be revealed in nominal field-charge-density relation as shown in Fig. 6(d). After the nominal electric field reaches point b, it will drop sharply. The maximum value of nominal electric field is taken to be the nominal breakdown strength of the nanocomposites.

The ultimate breakdown path of other four distribution cases and the nominal field-charge-density relation of all five cases is shown in Fig. 7 and Fig. 8(a). The conductive channels start at some local regions of significant electric field concentration, and then percolate and eventually become a major breakdown path in nanocomposite. The breakdown paths appear curved, due to the process of conductive channel selection except for case V of which $z_m = 13.51$. It is the most ideal distribution for that the distance among all particles is same, which results in a straight line breakdown path as shown in Fig. 7(d). Comparing the nominal field-charge-density relation of all these five cases in Fig. 8(a), it can be easily figured out that as the value of z_m increases, the nanocomposite appears stronger against breakdown. The nominal breakdown strength of which $z_m = 13.51$ is more than two times of which $z_m = -1.51$. It is noting that the final nominal charge density of the case of which $z_m = -1.51$ is larger than that of which $z_m = 3.99$ and 4.93. It is mainly because that before the establishment of a dominant breakdown path, the choice of local conductive channels of the aggregated distributed case is much more than that ordered ones. This will generate a lot of branches of conductive channel, thus can dissipate the extra energy during breakdown process. Still, the nominal breakdown resistance of which $z_m = -1.51$is lower than other cases. The breakdown strength is plotted against z_m in Fig. 8(b). It clearly shows that as the value of z_m increases, the breakdown strength can be enhanced tremendously.

Our quantitative method for describing distribution discussed

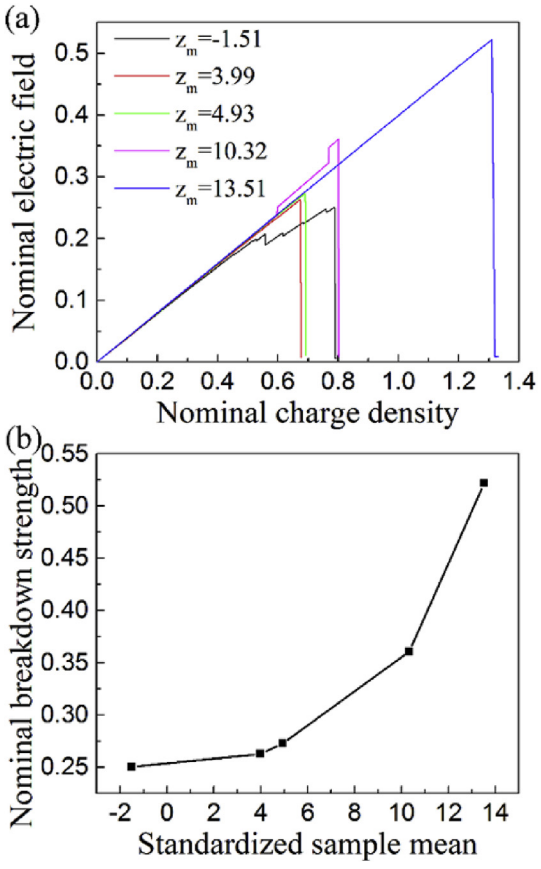

Fig. 8. (a) The nominal field-charge-density relation of all five cases. (b) The relation of nominal breakdown strength against z_m.

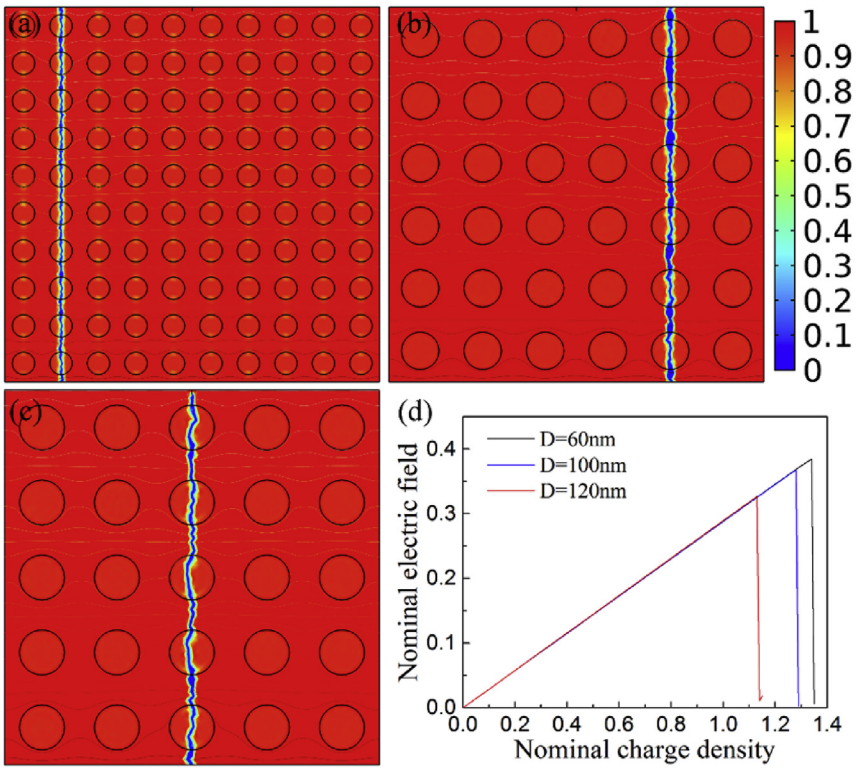

Fig. 9. The breakdown path images of which the diameters (D) are (a) 60 nm, (b) 100 nm and (c) 120 nm. The contour lines are the equipotential lines of the then-current electric field. (d) The nominal field-charge-density relation of all these three types.

above consider only the center of ceramic particles since we assume all particles are approximate in same size. To verify the size effect on the distribution of ceramic particles in polymer matrix, three types of ideally distributed nanoparticles with different diameter of particles has also been calculated using the same method above. The BT content of three types should be kept equal, thus the diameter and the amount of particles are well designed as shown in Fig. 9(a) to (c). The diameters of three types are set as 60 *nm*, 100 nm and 120 nm corresponding to the particles amount of 100, 36 and 25, which guarantees the same ideal distribution of ceramic particles under the same BT content. All three conditions of nanocomposites show straight line breakdown path similar to that in Fig. 7(d). The nominal field-charge-density relation of all these three types as seen in Fig. 9(d) indicates that the larger the ceramic particles, the lower the breakdown strength. It is because that under the same BT content, the local electric field of the larger size of ceramic particles concentrates more seriously [21].

4. Conclusion

A quantified method has been introduced in this work to describe the distribution of ceramic nanoparticles in polymer matrix based on Clark-Evans test and the quantified criterion (z_m) is defined to evaluate the distribution. As the value of z_m increases, the nanocomposite dielectric response on the contrary reduces slightly due to the concentration of local electric field. However, the nanocomposite of which the distribution of BT particles with larger z_m can hold better dielectric stability up to a higher level of applied electric field and then drop sharply at a critical applied electric field. The results of phase field simulation of breakdown process indicate that for the distribution of the same size ceramic particles, as the value of z_m increases, the nanocomposite turn out difficult to breakdown and the nominal breakdown strength of which $z_m = 13.51$ is more than two times of which $z_m = -1.51$. Summarization to the size effect on the distribution of ceramic particles is that the larger the ceramic particles, the lower the breakdown strength with the same ideal distribution of ceramic particles under the same content.

Acknowledgment

The work was supported by Ministry of Sciences and Technology of China through National Basic Research Program of China (973 Program 2015CB654604), National Natural Science Foundation of China (Grant No. 51272123, 51672148), and also supported by CBMI Construction Co., Ltd. In addition, our work is completed on the "Explorer 100" cluster system of Tsinghua National Laboratory for Information Science and Technology.

References

[1] L. Zhang, X. Shan, P. Bass, Y. Tong, T.D. Rolin, C.W. Hill, J.C. Brewer, D.S. Tucker, Z.Y. Cheng, Process and microstructure to achieve ultra-high dielectric constant in ceramic-polymer composites, Sci. Rep. 6 (2016) 35763.
[2] Q. Li, K. Han, M.R. Gadinski, G. Zhang, Q. Wang, High energy and power density capacitors from solution-processed ternary ferroelectric polymer nanocomposites, Adv. Mater. 26 (2014) 6244–6249.
[3] Z.-M. Dang, J.-K. Yuan, S.-H. Yao, R.-J. Liao, Flexible nanodielectric materials with high permittivity for power energy storage, Adv. Mater. 25 (2013) 6334–6365.
[4] C. Yang, H. Wei, L. Guan, J. Guo, Y. Wang, X. Yan, X. Zhang, S. Wei, Z. Guo, Polymer nanocomposites for energy storage, energy saving, and anticorrosion, J. Mater. Chem. A 3 (2015) 14929–14941.
[5] B.C. Riggs, S. Adireddy, C.H. Rehm, V.S. Puli, R. Elupula, D.B. Chrisey, Polymer nanocomposites for energy storage applications, Mater. Today Proc. 2 (2015) 3853–3863.
[6] G. Landi, A. Sorrentino, F. Fedi, H.C. Neitzert, S. Iannace, Cycle stability and dielectric properties of a new biodegradable energy storage material, Nano Energy 17 (2015) 348–355.
[7] Q. Chen, Y. Shen, S. Zhang, Q.M. Zhang, Polymer-based dielectrics with high energy storage density, Annu. Rev. Mater. Res. 45 (2015) 433–458.

[8] X. Hao, A review on the dielectric materials for high energy-storage application, J. Adv. Dielectr. 03 (2013) 1330001.
[9] Q. Wang, L. Zhu, Polymer nanocomposites for electrical energy storage, J. Polym. Sci. Part B Polym. Phys. 49 (2011) 1421–1429.
[10] S. Liu, S. Xiu, B. Shen, J. Zhai, L. Kong, Dielectric Properties, Energy Storage, Densities of poly(vinylidenefluoride) nanocomposite with surface hydroxylated cube shaped $Ba_{0.6}Sr_{0.4}TiO_3$ nanoparticles, Polymers 8 (2016) 45.
[11] X. Zhang, Y. Shen, Q. Zhang, L. Gu, Y. Hu, J. Du, Y. Lin, C.W. Nan, Ultrahigh energy density of polymer nanocomposites containing $BaTiO_3$@TiO_2 nanofibers by atomic-scale interface engineering, Adv. Mater. 27 (2015) 819–824.
[12] Y. Shen, Y. Hu, W. Chen, J. Wang, Y. Guan, J. Du, X. Zhang, J. Ma, M. Li, Y. Lin, Modulation of topological structure induces ultrahigh energy density of graphene/$Ba_{0.6}Sr_{0.4}TiO_3$ nanofiber/polymer nanocomposites, Nano Energy 18 (2015) 176–186.
[13] S. Liu, S. Xiao, S. Xiu, B. Shen, J. Zhai, Z. An, Poly (vinylidene fluoride) nanocomposites capacitors with significantly enhanced dielectric constant and energy density by filling with surface-fluorinated $Ba_{0.6}Sr_{0.4}TiO_3$ nanofibers, Rsc Adv. 5 (2015) 40692–40699.
[14] S. Liu, J. Zhai, J. Wang, S. Xue, W. Zhang, Enhanced energy storage density in poly(vinylidene fluoride) nanocomposites by a small loading of suface-hydroxylated $Ba_{0.6}Sr_{0.4}TiO_3$ nanofibers, ACS Appl. Mater. Interfaces 6 (2014) 1533–1540.
[15] P. Hu, Y. Shen, Y. Guan, X. Zhang, Y. Lin, Q. Zhang, C.-W. Nan, Topological-Structure modulated polymer nanocomposites exhibiting highly enhanced dielectric strength and energy density, Adv. Funct. Mater. 24 (2014) 3172–3178.
[16] P. Hu, Y. Song, H. Liu, Y. Shen, Y. Lin, C.-W. Nan, Largely enhanced energy density in flexible P(VDF-TrFE) nanocomposites by surface-modified electrospun $BaSrTiO_3$ fibers, J. Mater. Chem. A 1 (2013) 1688–1693.
[17] S. Rajesh, K. Sonoda, A. Uusimaki, K.H. Yang, H.Y. Lu, H. Jantunen, Effective dielectric response of polymer composites with ceramic coated silver flakes, J. Mater. Sci. Mater. Electron. 24 (2012) 191–195.
[18] L. Xie, X. Huang, C. Wu, P. Jiang, Core-shell structured poly(methyl methacrylate)/$BaTiO_3$ nanocomposites prepared by in situ atom transfer radical polymerization: a route to high dielectric constant materials with the inherent low loss of the base polymer, J. Mater. Chem. 21 (2011) 5897–5906.
[19] Kim Philseok, Natalie M. Doss, John P. Tillotson, Peter J. Hotchkiss, Ming-Jen Pan, Seth R. Marder, Jiangyu Li, Jeffery P. Calame, Joseph W. Perry, High energy density nanocomposites based on surface-modified $BaTiO_3$ and a ferroelectric polymer, Acs Nano 3 (2009) 2581–2592.
[20] Q. Zhang, F. Gao, C. Zhang, L. Wang, M. Wang, M. Qin, G. Hu, J. Kong, Enhanced dielectric tunability of $Ba_{0.6}Sr_{0.4}TiO_3$/Poly (vinylidene fluoride) composites via interface modification by silane coupling agent, Compos. Sci. Technol. 129 (2016) 93–100.
[21] Y. Hao, X. Wang, K. Bi, J. Zhang, Y. Huang, L. Wu, P. Zhao, K. Xu, M. Lei, L. Li, Significantly enhanced energy storage performance promoted by ultimate sized ferroelectric $BaTiO_3$ fillers in nanocomposite films, Nano Energy 31 (2017) 49–56.
[22] G. Zhang, D. Brannum, D. Dong, L. Tang, E. Allahyarov, S. Tang, K. Kodweis, J.-K. Lee, L. Zhu, Interfacial polarization-induced loss mechanisms in polypropylene/BaTiO3Nanocomposite dielectrics, Chem. Mater. 28 (2016) 4646–4660.
[23] S. Luo, S. Yu, R. Sun, C.P. Wong, Nano Ag-deposited BaTiO3 hybrid particles as fillers for polymeric dielectric composites: toward high dielectric constant and suppressed loss, ACS Appl. Mater. Interfaces 6 (2014) 176–182.
[24] H. Tang, H.A. Sodano, Ultra high energy density nanocomposite capacitors with fast discharge using $Ba_{0.2}Sr_{0.8}TiO_3$ nanowires, Nano Lett. 13 (2013) 1373–1379.
[25] J. Guan, C. Xing, Y. Wang, Y. Li, J. Li, Poly (vinylidene fluoride) dielectric composites with both ionic nanoclusters and well dispersed graphene oxide, Compos. Sci. Technol. 138 (2017) 98–105.
[26] K. Wu, C. Lei, W. Yang, S. Chai, F. Chen, Q. Fu, Surface modification of boron nitride by reduced graphene oxide for preparation of dielectric material with enhanced dielectric constant and well-suppressed dielectric loss, Compos. Sci. Technol. 134 (2016) 191–200.
[27] M. Donnay, S. Tzavalas, E. Logakis, Boron nitride filled epoxy with improved thermal conductivity and dielectric breakdown strength, Compos. Sci. Technol. 110 (2015) 152–158.
[28] X. Zhang, Y. Shen, B. Xu, Q. Zhang, L. Gu, J. Jiang, J. Ma, Y. Lin, C.W. Nan, Giant energy density and improved discharge efficiency of solution-processed polymer nanocomposites for dielectric energy storage, Adv. Mater. (2016).
[29] Z. Wang, J.K. Nelson, H. Hillborg, S. Zhao, L.S. Schadler, Dielectric constant and breakdown strength of polymer composites with high aspect ratio fillers studied by finite element models, Compos. Sci. Technol. 76 (2013) 29–36.
[30] Y. Song, Y. Shen, H. Liu, Y. Lin, M. Li, C.-W. Nan, Improving the dielectric constants and breakdown strength of polymer composites: effects of the shape of the BaTiO3 nanoinclusions, surface modification and polymer matrix, J. Mater. Chem. 22 (2012) 16491–16498.
[31] S.P. Fillery, H. Koerner, L. Drummy, E. Dunkerley, M.F. Durstock, D.F. Schmidt, R.A. Vaia, Nanolaminates: increasing dielectric breakdown strength of composites, ACS Appl. Mater. Interfaces 4 (2012) 1388–1396.
[32] N. Guo, S.A. DiBenedetto, P. Tewari, M.T. Lanagan, M.A. Ratner, T.J. Marks, Nanoparticle, size, shape, and interfacial effects on leakage current density, permittivity, and breakdown strength of metal oxide-polyolefin nanocomposites: experiment and theory, Chem. Mater. 22 (2010) 1567–1578.
[33] D. Tan, Y. Cao, E. Tuncer, P. Irwin, Nanofiller dispersion in polymer dielectrics, Mater. Sci. Appl. 04 (2013) 6–15.
[34] B. Luo, X. Wang, Y. Wang, L. Li, Fabrication, characterization, properties and theoretical analysis of ceramic/PVDF composite flexible films with high dielectric constant and low dielectric loss, J. Mater. Chem. A 2 (2014) 510–519.
[35] Y.U. Wang, D.Q. Tan, Computational study of filler microstructure and effective property relations in dielectric composites, J. Appl. Phys. 109 (2011) 104102.
[36] Y.U. Wang, Phase field model of dielectric and magnetic composites, Appl. Phys. Lett. 96 (2010) 232901.
[37] H.S. Khare, D.L. Burris, A quantitative method for measuring nanocomposite dispersion, Polymer 51 (2010) 719–729.
[38] M. Kulldorff, Tests of spatial randomness adjusted for an inhomogeneity: a general framework, J. Am. Stat. Assoc. 101 (2006) 1289–1305.
[39] P. Grabarnik, S. Chiu, Goodness-of-fit test for complete spatial randomness against mixtures of regular and clustered spatial point processes, Biometrika 89 (2002) 411–421.
[40] R. Assuncao, Testing spatial randomness by means of angles, Biometrics (1994) 531–537.
[41] D.L. Zimmerman, A bivariate Cramer-von Mises type of test for spatial randomness, Appl. Stat. (1993) 43–54.
[42] R. Hoffman, A.K. Jain, A test of randomness based on the minimal spanning tree, Pattern Recognit. Lett. 1 (1983) 175–180.
[43] J. Besag, P.J. Diggle, Simple Monte Carlo tests for spatial pattern, Appl. Stat. (1977) 327–333.
[44] P.J. Clark, F.C. Evans, Distance to nearest neighbor as a measure of spatial relationships in populations, Ecology 35 (1954) 445–453.
[45] T.E. Smith, Notebook on Spatial Data Analysis [online], 2016. http://www.seas.upenn.edu/~ese502/#notebook.
[46] Y.L. Wang, A.K. Tagantsev, D. Damjanovic, N. Setter, V.K. Yarmarkin, A.I. Sokolov, I.A. Lukyanchuk, Landau thermodynamic potential for BaTiO3, J. Appl. Phys. 101 (2007), 104115–104115-104119.
[47] K. Zhou, S.A. Boggs, R. Ramprasad, M. Aindow, C. Erkey, S.P. Alpay, Dielectric response and tunability of a dielectric-paraelectric composite, Appl. Phys. Lett. 93 (2008) 3.
[48] K. Zhou, S. Boggs, in: 2009 IEEE Pulsed Power Conference, IEEE, 2009, pp. 342–345.
[49] W. Hong, K.C. Pitike, Modeling breakdown-resistant composite dielectrics, in: K. Volokh, M. Jabareen (Eds.), Iutam Symposium on Mechanics of Soft Active Materials, Elsevier Science Bv, Amsterdam, 2015, pp. 73–82.
[50] K.C. Pitike, W. Hong, Phase-field model for dielectric breakdown in solids, J.Appl. Phys. 115 (2014) 8.
[51] S. Luo, Y. Shen, S. Yu, Y.-J. Wan, W.-H. Liao, R. Sun, C. Wong, Construction of 3d-$BaTiO_3$ network leading to significantly enhanced dielectric permittivity and energy storage density of polymer composites, Energy Environ. Sci. (2016).